

# Influence of laser wavelength instability, polarization fading and phase fluctuation on local heterodyne detection wavelength scanning BOTDR\*

LI Yongqian<sup>1,2,3</sup>, WANG Lei<sup>1,2,3\*\*</sup>, and FAN Haijun<sup>1,2,3</sup>

1. Department of Electronic and Communication Engineering, North China Electric Power University, Baoding 071003, China

2. Hebei Key Laboratory of Power Internet of Things Technology, North China Electric Power University, Baoding 071003, China

3. Baoding Key Laboratory of Optical Fiber Sensing and Optical Communication Technology, North China Electric Power University, Baoding 071003, China

(Received 16 October 2022; Revised 17 December 2022)

©Tianjin University of Technology 2023

In this paper, the influence of laser wavelength instability, polarization fading and phase fluctuation on local heterodyne detection wavelength scanning Brillouin optical time domain reflectometer (WS-BOTDR) is theoretically analyzed, and a local heterodyne detection WS-BOTDR system is built for experimental verification. The experimental results show that with the increase of sensing distance, the adverse effect of laser wavelength instability, polarization fading and phase fluctuation on local heterodyne detection WS-BOTDR is gradually aggravated, which will lead to the broadening and distortion of the wavelength power spectrum (WPS), resulting in large errors in demodulated Brillouin central wavelength (BCW) and temperature. The average temperature measurement errors at the positions of 1 km, 5 km, 9 km non-heating section and 9.45 km heating section are 1.76 °C, 3.42 °C, 3.89 °C and 4.3 °C, respectively.

**Document code:** A **Article ID:** 1673-1905(2023)04-0200-5

**DOI** <https://doi.org/10.1007/s11801-023-2176-0>

Brillouin optical time domain reflectometer (BOTDR), one of the most significant Brillouin-based distributed optical fiber sensors (B-DOFSs), has been widely applied in safety monitoring of oil and gas pipelines, health testing of large structures, owing to its superiority of single-ended measurement, simple structure and easy laying<sup>[1-4]</sup>. The basic principle of classical BOTDR is to detect the spontaneous Brillouin scattering (SPBS) light induced by the pulsed light injected from one end of the fiber. The Brillouin power spectrum (BPS) can be rebuilt by extracting the corresponding signal power at specific frequencies, and the Brillouin frequency shift (BFS) along the fiber can be determined by Lorentz fitting. As a result, the linear relationship between the BFS and the strain or temperature can be used to implement distributed strain or temperature sensing<sup>[5]</sup>.

The optical frequency difference scanning method<sup>[6-8]</sup> and the electric frequency difference scanning method<sup>[9-11]</sup> are the most widely utilized techniques for scanning the BPS. However, the optical frequency difference scanning method is susceptible to modulation

instability and harmonic noise of the modulator, and the self-beating frequency noise generated by the modulation is close to the difference frequency signal, which will interfere with the detected signal. Moreover, the electric frequency difference scanning method is over-reliant on the high flatness of detector gain response. To address the issues mentioned above, recently, a wavelength scanning method based on the wavelength dependence of BFS was proposed to accomplish the scanning of the BPS<sup>[12]</sup>. Since the SPBS signal is faint and difficult to detect, local heterodyne detection, where the SPBS light is coherent with local reference light, is usually adopted in the wavelength scanning BOTDR (WS-BOTDR) system to boost signal intensity. Nevertheless, the Brillouin scattering light produced by injected pulse pump light at each scattering point of the fiber and the local reference light generally have an unavoidable fiber length delay in the WS-BOTDR system based on local heterodyne detection. Consequently, the wavelength drift caused by the laser wavelength instability<sup>[13]</sup>, the polarization fading induced by the polarization mismatch<sup>[14]</sup> and the phase

\* This work has been supported by the National Natural Science Foundation of China (Nos.52177141, 62171185 and 61775057), the Natural Science Foundation of Hebei Province of China (Nos.F2019502112 and E2020502010), the Fundamental Research Funds for the Central Universities (Nos.2019MS086 and 2017MS112), and the S&T Program of Hebei, China (No.SZX2020034).

\*\* E-mail: hdbdwl@163.com

fluctuation resulted from the transmission of the fiber link will lead to the coherence degradation of the heterodyne signal and the distortion of the BPS<sup>[15]</sup>, thereby diminishing the measurement accuracy and sensing distance.

The principle of WS-BOTDR is based on the wavelength dependence of BFS. In the range of (1 550±15) nm, BFS is linearly decreased with the increase of the center wavelength, and the relationship between them is shown in Eq.(1), where  $V_A$  is the speed of sound in the fiber, and  $n$  is the refractive index of the fiber.

$$v_B = \frac{2V_A n}{\lambda_p} \quad (1)$$

The relationship between wavelength and BPS is depicted in Fig.1. It can be known from Fig.1 that WS-BOTDR is to fix a certain frequency  $\nu_f$  that usually the BFS at room temperature on the BPS, by changing the wavelength  $\lambda$  and then collecting the power  $g(\lambda)$  corresponding to the frequency  $\nu_f$  of the power spectrum, the wavelength power spectrum (WPS) curve can be obtained in Fig.2, which can be expressed as Lorentz function as follows

$$g(\lambda) = g_0 \frac{(\Delta\lambda/2)^2}{(\lambda - \lambda_p)^2 + (\Delta\lambda/2)^2}, \quad (2)$$

where  $g_0$  is the peak value of the WPS,  $\Delta\lambda$  is the WPS linewidth, and  $\lambda_p$  is the central wavelength corresponding to the peak of the WPS curve, called Brillouin central wavelength (BCW).

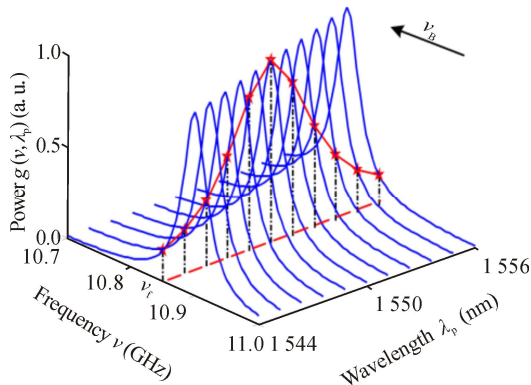


Fig.1 Relationship between wavelength and BPS

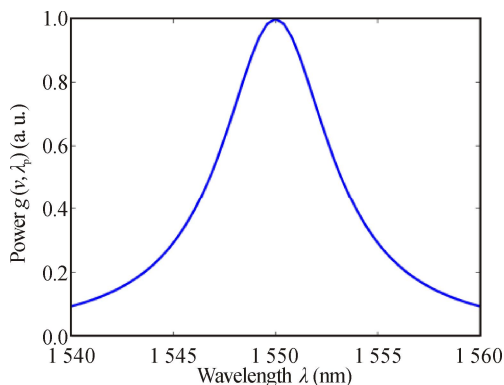


Fig.2 Wavelength power spectrum

Assuming that the temperature of fiber varies from  $T_0$  to  $T$ , temperature variable is  $\Delta T$ , the corresponding BFS changes from  $\nu_B$  to  $\nu_B'$ , and the BCW changes from  $\lambda_p$  to  $\lambda_p'$ . The temperature  $T$  can be demodulated from the changed BCW  $\lambda_p'$ , BFS wavelength dependence coefficient  $C$  and BFS temperature dependence coefficient  $C_T$  that changes slightly in the range of (1 550±15) nm, and can be considered to be basically unchanged<sup>[16]</sup>:

$$T = T_0 + \Delta T = T_0 + \frac{(\nu_B' - \nu_B)}{C_T} = T_0 + \frac{C(\lambda_p' - \lambda_p)}{C_T} \quad (3)$$

The schematic diagram of local heterodyne detection WS-BOTDR is shown in Fig.3. The signal of heterodyne detection in photoelectric detector (PD) is the Brillouin scattering light produced by the injected pulse light of the fiber at the time  $t_0$  and the reference light output from the light source at time  $t_0 + 2nz/c$ , respectively.

The Stokes scattered light returning to the front of the fiber and the local reference light from the laser source that encounters and interferes with the Stokes light can be expressed as

$$E_S(t) = E_S[\cos\theta_S(t_0 + 2nz/c)] \times \exp\left\{2\pi i \left[ \frac{c}{\lambda_0(t_0)} - \frac{2nV_A}{\lambda_0(t_0)} \right] t + i\varphi_S(t_0 + 2nz/c) + i\varphi_N(t_0 + 2nz/c)\right\}, \quad (4)$$

$$E_L(t) = E_L[\cos\theta_L(t_0 + 2nz/c)] \times \exp\left\{i \left[ 2\pi \frac{c}{\lambda_0(t_0 + 2nz/c)} t + \varphi_L(t_0 + 2nz/c) \right]\right\}, \quad (5)$$

where  $E_S$  and  $E_L$  are the intensities of Stokes light and local reference light, respectively,  $\lambda_0(t_0)$  is the center wavelength of the pulsed light injected into the fiber at time  $t_0$ ,  $\lambda_0(t_0 + 2nz/c)$  is the center wavelength of local reference light at time  $t_0 + 2nz/c$ ,  $t_0$  is the initial time when the pulsed light reaches the beginning of the fiber,  $2nz/c$  denotes the delay difference between the injected pulsed light and the Brillouin scattered light from the scattering point  $z$ , and  $c$  is the speed of light.  $\cos\theta_S(t_0 + 2nz/c)$  and  $\cos\theta_L(t_0 + 2nz/c)$  are polarization correlation factors of Stokes light and local reference light at time  $t_0 + 2nz/c$ ,  $\varphi_S(t_0 + 2nz/c)$  and  $\varphi_L(t_0 + 2nz/c)$  are the phases of Stokes light and local reference light at time  $t_0 + 2nz/c$ , respectively, and  $\varphi_N(t_0 + 2nz/c) = 2\pi z\beta f_S$  is the phase fluctuation generated during fiber transmission, where  $\beta$  and  $f_S$  are the group delay and frequency of Stokes light, respectively.

Provided that the PD has a suitable band-pass filtering characteristic, the direct current term and the sum frequency term in the heterodyne detection are filtered out, and the photocurrent of the heterodyne detection output from the PD is

$$i_{LS}(t) = 2R\sqrt{P_L P_S} [\cos\theta(t_0 + 2nz/c)] \times \exp\left\{2\pi i \frac{2nV_A}{\lambda_0(t_0)} t + 2\pi i \left[ \frac{c}{\lambda_0(t_0 + 2nz/c)} - \frac{c}{\lambda_0(t_0)} \right] t + \right\}$$

$$i\varphi_{LS}(t_0 + 2nz/c) - i\varphi_N(t_0 + 2nz/c)\}, \quad (6)$$

in which  $R$  is the responsivity of PD,  $P_S$  and  $P_L$  are the power of Stokes light and local reference light, respectively, and  $\cos\theta(t_0 + 2nz/c)$  and  $\varphi_{LS}(t_0 + 2nz/c)$  are the polarization correlation factor and the phase difference between Stokes light and local reference light at time  $t_0 + 2nz/c$  after heterodyne. It can be seen from Eq.(6) that the polarization fading is reflected on  $\cos\theta$ , that is, when the polarization state of Stokes light coincides with the local reference light,  $\cos\theta$  is 1, while when they are orthogonal,  $\cos\theta$  is 0. The amplitude of heterodyne signal will fluctuate due to the randomness of polarization state, and in severe cases, the signal may be submerged in the noise. The term  $c/\lambda_0(t_0 + 2nz/c) - c/\lambda_0(t_0)$  illustrates the effect of the laser wavelength instability, which causes drift in the measured BCW.  $\varphi_N(t_0 + 2nz/c)$  can be used to characterize the effect of phase fluctuation caused by fiber transmission on local heterodyne signal. Because the optical fiber is very sensitive to temperature and vibration variations applied to it, which causes the refraction index variations, so the group delay  $\beta$  as well as  $\varphi_N$  changes randomly. It results in that each signal used for superposition averaging is obtained by different phase differences between Stokes and local reference light, thus distorting the average curve, especially when a large number of superposition averaging times are needed to improve the signal-to-noise ratio (SNR).

To verify the correctness of theoretical analysis, the WS-BOTDR system based on local heterodyne detection is constructed for experimental verification. The experimental step is shown in Fig.3. The output light of the tunable laser with  $\sim 100$  kHz linewidth and 12.8 dBm output power is divided into two branches by 50: 50 Coupler 1. The upper branch is modulated to pulsed signal light with a repetition rate of 10 kHz and width of 130 ns by a high extinction ratio electro-optic modulator (EOM), driven by a pulse generator (PG). Then the pulsed signal light is amplified by an erbium-doped fiber amplifier 1 (EDFA1) and filtered by a tunable optical filter 1 (TOF1). After being attenuated by the variable optical attenuator 1 (VOA1), the pulsed signal light enters the fiber under test (FUT) through an optical circulator to generate SPBS. The lower branch, which acts as the local reference light, and the Brillouin scattered light return from the FUT that is amplified by EDFA2 and filtered by TOF2 to filter out Rayleigh scattered light, anti-Stokes scattered light and amplified spontaneous emission (ASE) noise are coupled in Coupler 2, after then, entering the PD with a bandwidth of 11.9 GHz for local heterodyne detection. The peak pulse power injected at the beginning of the fiber is 100 mW and the power input to PD is 400  $\mu$ W after adjusted by VOA2 and VOA3.

A standard single-mode fiber with 9.5 km is employed in the experiment. The relevant parameters are calibrated before the experiment. The BFS of the fiber is 10.847 GHz and the corresponding BCW is 1 550.12 nm at a room temperature of 27.6 °C. The wavelength de-

pendence coefficient of BFS is  $-7.33$  MHz/nm and the temperature dependence coefficient of BFS is  $1.07$  MHz/°C. In the experiment, about 50-m-long fiber near the far end is placed in a thermostatic water bath and heated to 50 °C. The electrical spectrum analyzer (ESA) with a center frequency of 10.847 GHz operated in "zero-span" mode is used to measure the power traces along the FUT at different scanning wavelengths. The wavelength of the tunable laser is scanned from 1 542.12 nm to 1 561.32 nm, which can cover the temperature measurement range of about 80 °C. The wavelength scanning step is selected as 0.8 nm, corresponding to the BFS about 5.6 MHz, so that the power spectrum data will not be lost and the measurement efficiency can be guaranteed. The power traces at each wavelength are averaged 5 000 times to improve SNR.

The 3D power spectrum is shown in Fig.4. It can be seen that the shift of BCW in the heating section is not obvious. In order to more clearly explain the influence of laser wavelength instability, polarization fading and phase fluctuation on local heterodyne detection WS-BOTDR, we perform a Lorentz fit on the WPS at different fiber positions. The BCW, the linewidth and the demodulated temperature along the fiber are obtained, as shown in Fig.5(a), (b) and (c).

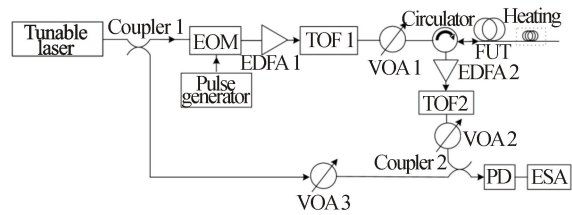


Fig.3 Local heterodyne detection WS-BOTDR system

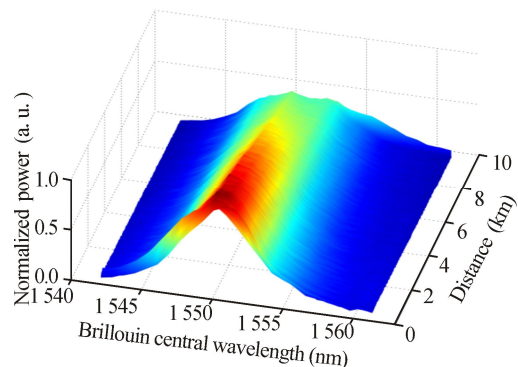
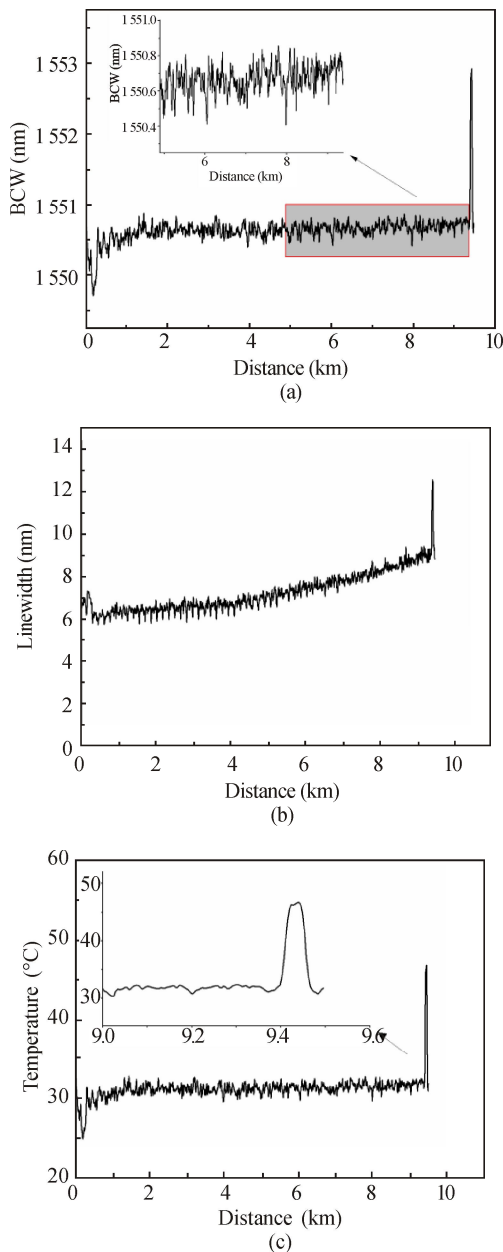


Fig.4 3D power spectrum

From Fig.5(a) and (b), it can be seen that when the sensing distance is relatively short, that is, less than 4 km, the detrimental effects of laser wavelength instability, polarization fading and phase fluctuation are relatively slight. Consequently, the measured BCW and power spectrum linewidth are basically stable. As the sensing distance increases, the time delay difference between local reference light and Brillouin signal light becomes more significant, and the influence of laser wavelength

instability, polarization fading and phase fluctuation is strengthened. As a result, the BCW and power spectral linewidth measured in the non-heating section begin to drift along with sensing distance. These result in a larger average BCW of 1 550.619 nm in non-heating section, and the temperature demodulated by Eq.(3) is 31 °C, the average measurement error is 3.4 °C. Moreover, the heating section is at the end of the fiber, so it is more seriously affected by the above three effects, and the average measurement error is 4.3 °C.



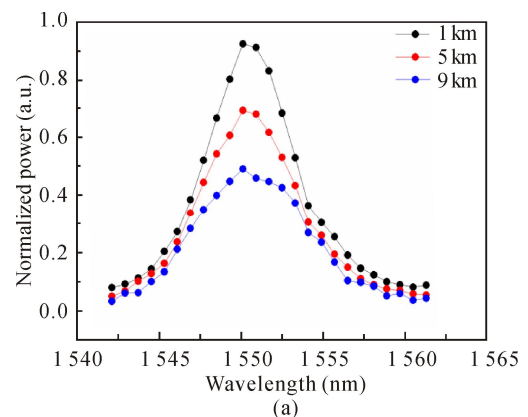
**Fig.5 (a) BCW, (b) linewidth and (c) demodulated temperature along the fiber**

In the local heterodyne detection, there is a time delay difference between the local reference light and the Brillouin signal light. The detected Brillouin spectrum is composed of Brillouin scattering spectra with different

center wavelengths and round-trip times at different fiber positions. The coherence of Brillouin scattered light generated at the sensing distance  $z$  and local reference light is affected by laser wavelength instability, polarization fading and phase fluctuation. And the longer the sensing distance, the larger the delay difference, the more serious the above effect. It will lead to coherence deterioration of heterodyne signal, distortion and broadening of WPS with heterodyne detection, which will cause serious impact on the subsequent Lorentz fitting and the measurement of the BCW, thus deteriorating the measurement accuracy.

To demonstrate the point, we extract the WPS and relevant parameters of the non-heating section at the positions of 1 km, 5 km, 9 km and 9.45 km heating section, as shown in Fig.6 and Tab.1. Fig.6(a) shows that as the increase of the sensing distance, the WPS is gradually broadened, resulting in a gradual increase in the linewidth, the linewidths obtained by fitting power spectrum at the positions of 1 km, 5 km, 9 km are 6.19 nm, 7.18 nm and 9.01 nm, respectively, as given in Tab.1. Besides, the spectral pattern gradually deviates from the ideal Lorentz spectrum, the WPS with a sensing distance of 9 km is distorted, and the fitting degrees  $R^2$  at the positions of 1 km, 5 km, 9 km are 0.995 2, 0.993 3, 0.982 8, respectively. Therefore, the average temperature measurement errors of 1 km, 5 km and 9 km increase gradually, which are 1.76 °C, 3.42 °C and 3.89 °C, respectively. In order to eliminate the influence of randomness and ensure consistency, the average error is calculated using about 50 m data near each location, which is consistent with the length of heating section. Furthermore, the distortion and broadening of heating section are especially serious as can be seen from Fig.6(b), and the linewidth and  $R^2$  obtained by fitting are 12.50 nm and 0.949 0, which is the reason for the large average temperature measurement error of 4.3 °C.

In summary, the influence of laser wavelength instability, polarization fading and phase fluctuation on local heterodyne detection WS-BOTDR is theoretically analyzed and experimentally verified. The results indicate that as the sensing distance increases, the influence of laser wavelength instability, polarization fading and



(a)

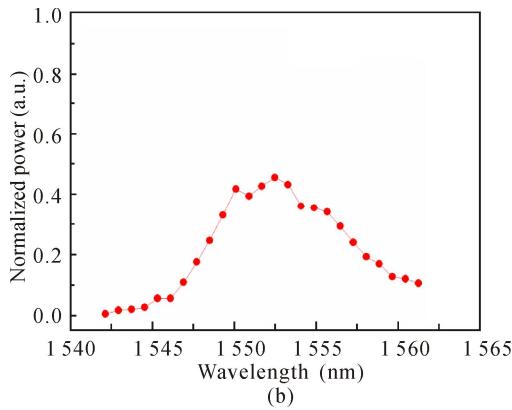


**Fig.6 WPS at the positions of (a) 1 km, 5 km, 9 km fiber lengths and (b) 9.45 km heating section**

**Tab.1 Relevant parameters at different positions**

	1 km	5 km	9 km	9.45 km
Linewidth (nm)	6.19	7.18	9.01	12.5
$R^2$	0.995 2	0.993 3	0.982 8	0.949 0
BCW (nm)	1 550.378	1 550.620	1 550.688	1 552.856
Error (°C)	1.76	3.42	3.89	4.3

phase fluctuation on local heterodyne detection WS-BOTDR becomes more and more serious, which will lead to WPS distortion and linewidth broadening, thus the BCW and the demodulated temperature will produce a large error. The average temperature measurement errors of the non-heating section and the heating section are 3.4 °C and 4.3 °C, respectively.

**Statements and Declarations**

The authors declare that there are no conflicts of interest related to this article.

**References**

[1] BAO X Y, ZHOU Z C, WANG Y. Review: distributed time-domain sensors based on Brillouin scattering and FWM enhanced SBS for temperature, strain and acoustic wave detection[J]. *Photonix*, 2021, 2(1): 14.

[2] SUN J X, ZHANG Z G, LI Y M, et al. Distributed transmission line ice-coating recognition system based on BOTDR temperature monitoring[J]. *Journal of lightwave technology*, 2021, 39(12): 3967-3973.

[3] GAO L, CAO Y, LIU H L, et al. Experiment and numerical study on the monitoring of super long cast-in-place pile temperature based on BOTDR technology[J]. *Measurement*, 2021, 179: 109481.

[4] LIN R, ZHU Y F, TIAN L, et al. On-situ monitoring of sleet-thawing for OPGW based on long distance BOTDR[J]. *Optoelectronics letters*, 2021, 17(4): 226-230.

[5] LI Y Q, FAN H J, ZHANG L X, et al. Single-mode input fiber combined with multimode sensing fiber used in Brillouin optical time-domain reflectometry[J]. *Photonics*, 2022, 9(6): 398.

[6] LI Y Q, FAN H J, ZHANG L X, et al. A bend-tolerant BOTDR distributed fiber sensor[J]. *Optics communications*, 2022, 514: 128110.

[7] LI Y Q, FAN H J, WANG L, et al. Bend-tolerant fiber sensor based on BOTDR system[J]. *Optoelectronics letters*, 2022, 18(06): 343-348.

[8] FU G W, CAO J Q, LI W L, et al. A novel positioning and temperature measurement method based on optical domain demodulation in the BOTDR system[J]. *Optics communications*, 2021, 480: 126490.

[9] WANG Q L, BAI Q, LIANG C S, et al. Random coding method for SNR enhancement of BOTDR[J]. *Optics express*, 2022, 30(7): 11604-11618.

[10] WAN D, SHAN L N, XI L X, et al. An improved Lorentz fitting algorithm for BOTDR using SVM model to capture the main peak of power cumulative average data[J]. *Optical fiber technology*, 2022, 74: 103082.

[11] LI W, JIANG L, ZHANG T F, et al. Brillouin frequency estimation in distributed Brillouin optical fiber sensors based on instantaneous frequency[J]. *IEEE sensors journal*, 2022, 22(19): 18501-18507.

[12] ZORNOZA A, OLIER D, SAGUES M, et al. Brillouin spectral scanning using the wavelength dependence of the frequency shift[J]. *IEEE sensors journal*, 2011, 11(2): 382-383.

[13] LI Y Q, LI X J, AN Q, et al. Detrimental effect elimination of laser frequency instability in Brillouin optical time domain reflectometer by using self-heterodyne detection[J]. *Sensors*, 2017, 17(3): 634.

[14] HAO Y Q, YANG K, LIU N N, et al. Suppression of amplitude fluctuation in Brillouin optical fiber reflectometry employing polarization beam splitter and pre-amplification technique[J]. *Optical fiber technology*, 2020, 57: 102217.

[15] LI Z L, YAN L S, SHAO L Y, et al. Precise Brillouin gain and phase spectra measurements in coherent BOTDA sensor with phase fluctuation cancellation[J]. *Optics express*, 2016, 24(5): 4824-4833.

[16] LI W, ZHU N H, WANG L X. Photonic phase shifter based on wavelength dependence of Brillouin frequency shift[J]. *IEEE photonics technology letters*, 2011, 23(14): 1013-1015.